Journal of Rock Mechanics and Geotechnical Engineering 18 (2026) 3852–3867

Contents lists available at ScienceDirect

Journal of Rock Mechanics and Geotechnical Engineering

journal homepage: www.jrmge.cn

Full Length Article

Instability mechanism of dangerous rock masses on bank slopes containing a single shear band under the deterioration of reservoir water

Xueyan Guo [a,b], Xinrong Liu [a,b,c,*], Jilu Zhang [a,b], Lojain Suliman [a,b], Xinyang Luo [a,b], Fuchuan Zhou [a,d]

[a] School of Civil Engineering, Chongqing University, Chongqing, 400045, China
[b] National Joint Engineering Research Center of Geohazards Prevention in the Reservoir Areas, Chongqing University, Chongqing, 400045, China
[c] State Key Laboratory of Coal Mine Disaster Dynamics and Control, Chongqing University, Chongqing, 400045, China
[d] Chongqing Vocational Institute of Engineering, Chongqing, 402260, China

ARTICLE INFO

Article history:
Received 19 February 2025
Received in revised form
14 July 2025
Accepted 21 August 2025
Available online 13 December 2025

Keywords:
Three gorges reservoir area
Water–rock interaction
Shear band
Dangerous rock mass
Slope stability

ABSTRACT

Taking the Banbiyan dangerous rock mass as the focus, this study employs field investigations, model experiments, and numerical simulations to explore the instability mechanisms of dangerous rock masses on bank slopes containing a single shear band under the deterioration of reservoir water. The results indicate that the failure mode of the dangerous rock mass is collapse of rock mass in the hydro-fluctuation belt (HFB) – internal damage to the dangerous rock mass – development and through-going of fractures on both sides – sliding failure of the lower rock detaching from the parent rock. As the shear band gradually deteriorates, stress concentration develops around it near the highest water level. Within the rock mass close to the highest water level, a phenomenon of unloading occurs, and the pore water pressure at the shear band–bedrock interface eventually exceeds that within the rock mass of the HFB. In the numerical simulation, before 40 dry-wet cycles, the damage zone is concentrated near the shear band above the highest water level. Afterward, it concentrates around the fractures on both sides of the dangerous rock mass. The sensitivity of different shear band characteristics to the stability of the dangerous rock mass is ranked as follows: the height-length ratio of the shear band–bedrock interface, followed by the filling material thickness, dip angle, width, and degree of fragmentation. The findings can provide valuable reference for the stability and prevention of such dangerous rock masses.
© 2026 Institute of Rock and Soil Mechanics, Chinese Academy of Sciences. Published by Elsevier B.V. This is an open access article under the CC BY-NC-ND license (http://creativecommons.org/licenses/by-nc-nd/4.0/).

1. Introduction

The complex geological tectonic movements in the Three Gorges Reservoir area (TGRA) have given rise to the peaks and cliffs on both banks. Under the long-term unloading effect of the river water, numerous large-scale dangerous rock masses of varying types have appeared along both banks of the Wushan section (Liu et al., 2025). Due to the unique water storage method, the rock mass at the foot of the slopes in the reservoir area has undergone continuous dry-wet cycles (Fu, 2011), forming the hydro-fluctuation belt (HFB) nearly 30 m high. Over time, the deteriorating rock mass in the HFB has become a critical factor in the instability of these dangerous rock masses. Field investigations and existing literature (Yin et al., 2023; Liu et al., 2024) indicate that the Banbiyan dangerous rock mass (BDRM) within the Wushan section comprises four shear bands, characterized by substantial fragmentation and moderate width (Fig. 1). Notably, shear bands 1 and 2 are partially located within the HFB and have been subjected to prolonged dry-wet cycles. The continuous dry-wet cycling reduces the strength of both the shear band–bedrock interface and the infill materials within the shear band (Guo, 2021; Guo et al., 2025), thereby leading to a decline in the overall shear band strength, becoming the primary structural surfaces threatening the stability of the dangerous rock mass. Therefore,

* Corresponding author. School of Civil Engineering, Chongqing University, Chongqing, 400045, China.
E-mail address: liuxrong@126.com (X. Liu).
Peer review under responsibility of Institute of Rock and Soil Mechanics, Chinese Academy of Sciences.

https://doi.org/10.1016/j.jrmge.2025.08.042
1674-7755/© 2026 Institute of Rock and Soil Mechanics, Chinese Academy of Sciences. Published by Elsevier B.V. This is an open access article under the CC BY-NC-ND license (http://creativecommons.org/licenses/by-nc-nd/4.0/).

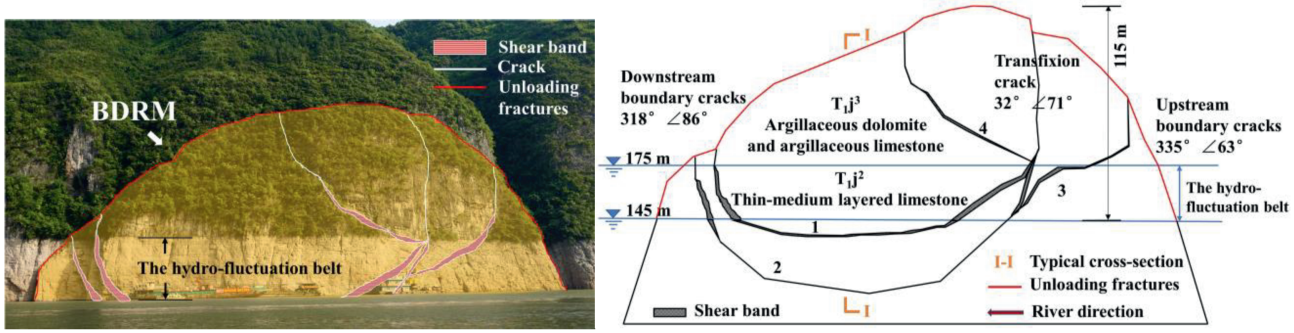


Fig. 1. BDRM and its geological characteristics.

elucidating the instability mechanisms of dangerous rock masses containing such shear bands under the deterioration of reservoir water is of great significance for the prevention and treatment of these dangerous rock masses.

Research concerning the stability of dangerous rock masses has become increasingly comprehensive, both domestically and internationally. The primary methods employed include field investigations, theoretical calculations, model tests, and numerical simulations. These studies have explored the classification of dangerous rock masses (Hungr et al., 2014), failure modes (Shi et al., 2023), and instability mechanisms (Zheng et al., 2013; Chen et al., 2015; Zhao et al., 2022). In light of the destabilizing effects posed by external loads, such as precipitation, excavation activities, and seismic events, numerous researchers have examined the failure mechanisms and energy evolution characteristics of dangerous rock masses subjected to such loads (Shi et al., 2020; Wang et al., 2024). In the unique hydrological environment of the TGRA, the deteriorating effect of reservoir water on rock masses has become a new factor influencing the stability of dangerous rock masses on both banks and has also gradually become a focal point of scholarly research. The reservoir area contains many types of dangerous rock masses, such as the columnar dangerous rock mass (e.g. Jianchuandong dangerous rock mass), the wedge-shaped dangerous rock mass (e.g. Qingyanzi dangerous rock mass), the arrayed columnar dangerous rock mass (e.g. Huangyanwo dangerous rock mass), and the plate-like dangerous rock mass (e.g. BDRM). Each type demonstrates distinct failure patterns under the influence of reservoir water (Liu et al., 2025). Currently, research on dangerous rock masses in the reservoir area has been primarily concentrated on columnar types. Scholars primarily employed methods such as field surveys (Yin et al., 2023), theoretical calculations (Wang et al., 2020a, 2023; Yin et al., 2022), model tests (Guo, 2021; Liu et al., 2023a), and numerical simulations (Wang et al., 2020b) to analyze the failure modes, static and dynamic stability, instability mechanisms, and control measures of columnar dangerous rock masses, providing valuable insights for the prevention and treatment of dangerous rock masses. Regarding the BDRM, scholars have primarily employed field surveys (Yin et al., 2023) and numerical simulations (Chen et al., 2022) to discuss the impact of HFB rock mass deterioration and precipitation on the stability of dangerous rock masses. However, the shear bands within this dangerous rock mass are likewise affected by the deteriorative influence of reservoir water. Further research is needed on the instability mechanism and failure mode of dangerous rock masses under shear band deterioration. Research by domestic and international scholars on interlayers has primarily focused on the impact of weak interlayers on the stability of soil slopes (Elkamhawy et al., 2018; Wei et al., 2020; Fan et al., 2024; Li et al., 2024). The occurrence of such shear bands in rock slopes is relatively rare, and there is a lack of literature on the effect of these shear bands on slope stability. Therefore, it is urgent to conduct research on the instability mechanisms of dangerous rock masses containing shear bands under the deterioration of reservoir water.

Due to existing differences in the morphology, degree of fragmentation, and extent of deterioration of the shear bands observed in the field, it is plausible that a single shear band may exert a dominant influence on the stability of the dangerous rock mass, or that multiple shear bands may act synergistically to affect overall stability. In addition, elucidating the impact of the deterioration of a single shear band on the stability of the dangerous rock mass serves as a prerequisite for investigating the combined effects of multiple shear bands. This paper only discusses the instability mechanisms of dangerous rock masses on bank slopes containing a single shear band under the deterioration of reservoir water. This provides the foundation for subsequent investigations into the impact of double shear bands on the stability of the dangerous rock mass. Based on this, field investigations are conducted to generalize typical dangerous rock mass models, and laboratory similarity model tests are carried out to clarify the instability evolution process, displacement characteristics, and internal stress variation patterns of dangerous rock masses on bank slopes containing a single shear band under the deterioration of reservoir water. Moreover, numerical simulations are used to reveal the displacement field, stress field, and fracture evolution patterns during the instability process. Finally, the sensitivity of shear band characteristics to the stability of dangerous rock masses is discussed to provide a theoretical basis for the monitoring and prevention of such dangerous rock masses in the reservoir area.

2. Model test design

2.1. Engineering geological background

The BDRM is located on the right bank of the Wushan section of the TGRA in Chongqing. The study area primarily consists of limestone of the Lower Triassic Jialingjiang Formation, overlaid by Quaternary colluvial soil. The BDRM is characterized by an anti-dip layered rock slope with a slope angle of 85° and bedding dip angles ranging from 2° to 24°. The HFB surface of the dangerous rock mass contains multiple vertical fractures, with individual fracture lengths reaching approximately 30 m and depths extending up to 7 m. The front edge of the slope is intersected by four shear bands, primarily generated due to unloading caused by river incision (Liu et al., 2024). Shear bands 1 and 2 have widths ranging from 0.5 m to 1.8 m, with dip angles of approximately 55°, and they extend below the water level. The unloading fractures at the rear edge of the bank slope have a strike of 318° and a dip angle of 86°, with

crack openings ranging from approximately 36 cm–65 cm. These fractures are connected from top to bottom with shear bands 1 and 2, which divide the slope into a single dangerous rock mass (Fig. 2). The location of the typical cross-section in the dangerous rock mass is shown in Fig. 1. The dangerous rock mass is exposed to water on three sides, with shear bands 1 and 2, located in the HFB, exposed on the outer side of the mass. These shear bands are relatively fragmented but exhibit clear layer structural characteristics, which have been subjected to long-term dry-wet cycles due to reservoir water. The deterioration of the shear bands involves the deterioration of structural surfaces and rock. The structural surface deterioration refers to the deterioration of the shear band–bedrock interface, while the rock deterioration refers to the degradation of the internal infill blocks. Since the shear bands within the HFB experience deterioration due to the influence of reservoir water, the upper shear bands are unaffected by the dry-wet cycles. The failure mechanism of dangerous rock masses on bank slopes in this context requires further in-depth research.

2.2. Objective and principle of the test

The main objective of the experiment conducted in this study is to simulate the deteriorating effect of reservoir water on the rock mass in the HFB (i.e. the impact of dry-wet cycles on the rock mass) and to explore the failure process of dangerous rock masses. This includes investigating the effect of shear band deterioration within the HFB on the stability of the dangerous rock mass, specifically focusing on the deterioration of the shear band–bedrock interface and the deterioration of the infill material within the shear band under the influence of reservoir water. A new bond material was introduced in the traditional similar material proportioning tests. This material can simulate the deteriorating effects of dry-wet cycles on the rock mass to some extent. Upon contact with water, this bond material undergoes hydrolysis and loses its adhesive properties over time, thus simulating the loss of strength of the structural surface and the rock, reflecting the degradation process of both the structural surface and the rock. This is a key step in the model test. It should be noted that this model experiment provides only a qualitative analysis of the failure process of the dangerous rock mass. The effects of water level fluctuations on the dangerous rock mass are not considered. The experiment uses a steady water-rise method, allowing the experimental materials to fully interact with water, causing the deterioration of the shear band–bedrock interface and the infill blocks within the shear band. The experiment aims to explore the changes in relative displacement and internal stress of the slope before and after the failure of the dangerous rock mass.

2.3. Test material design

To investigate the instability process of the dangerous rock mass, it is necessary to select similar materials and determine their proportion. First, the similarity ratio calculation of key physical and mechanical parameters of the dangerous rock mass is carried out using the third similarity law. The key physical quantities involved include 10 parameters, with the fundamental quantities being density (ρ), elastic modulus (E), and geometric dimensions (L), where the fundamental dimensions are [M], [L], and [T]. The results are shown in Table 1.

In the model test, three parts need to be simulated using similar materials: the dangerous rock mass, the internal infill rock blocks of the shear band, and the shear band–bedrock interface. Many scholars (Wang et al., 2020a; Liu et al., 2023a; Zhou et al., 2023) have focused primarily on the deformation of the dangerous rock mass when investigating its failure mode. In such studies, the bedrock is typically treated as a rigid body. In this test, the bedrock is also considered a rigid body, and for waterproofing considerations, it is decided that the bedrock will be constructed from brick and cement mortar. For the selection of similar materials for the dangerous rock mass, reference is made to the types of similar materials used in previous model tests (Xu et al., 2022), and it is determined that river sand, barite powder, gypsum, glycerin, and

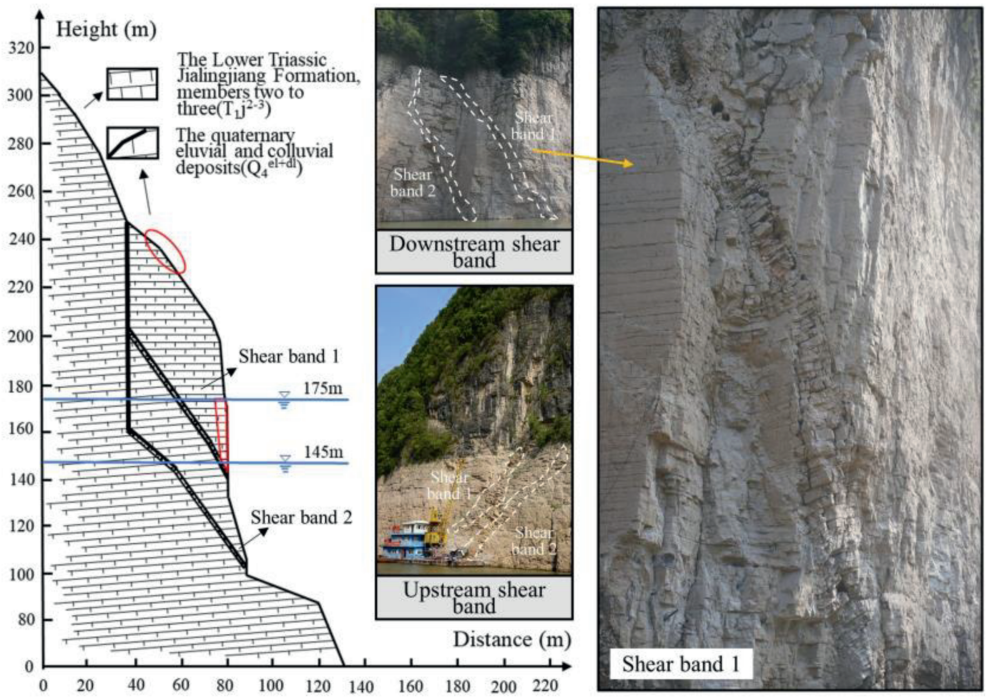


Fig. 2. Geological structure and shear band locations of the dangerous rock mass.

Table 1
Key physical and mechanical quantities and similarity coefficients.

Physical quantity	Dimension	Similarity ratio
Density	$[ML^{-3}]$	$C_\rho = 1$[a]
Elastic modulus	$[ML^{-1}T^{-2}]$	$C_E = 100$[a]
Geometric dimensions	[L]	$C_L = C_E^{0.5} C_\rho^{-0.5} C_t = 100$[a]
Cohesion	$[ML^{-1}T^{-2}]$	$C_c = C_E C_\varepsilon = 100$
Internal friction angle	–	$C_\varphi = 1$
Stress	$[ML^{-1}T^{-2}]$	$C_\sigma = C_E C_\varepsilon = 100$
Strain	–	$C_\varepsilon = C_\rho C_g C_L C_E^{-1} = 1$
Poisson's ratio	–	$C_\mu = 1$
Displacement	[L]	$C_u = C_L C_\varepsilon = 100$
Acceleration	$[LT^{-2}]$	$C_g = C_u C_t^{-2} = 1$

[a] The physical quantity corresponding to this similarity coefficient is adopted as the fundamental control quantity.

water will be used to simulate the properties of limestone. Following multiple mix ratio trials and validation through laboratory geotechnical testing, the final similar material mix is determined as river sand: barite powder: gypsum: glycerin: water = 1:0.388:0.241:0.037:0.185. The preparation of similar material for the dangerous rock mass is shown in Fig. 3. The corresponding prototype values, target values, and actual values of the similar material parameters are presented in Table 2.

In the selection of similar materials for the infill blocks within the shear band and the rock mass in the HFB, since the field shear band infill material and the rock mass in the HFB are limestone, the river sand and barite powder were chosen as aggregates. Gypsum and polyvinyl acetate emulsion (commonly known as white latex) were selected as the binder. In this case, polyvinyl acetate loses its strength upon contact with water, while gypsum hardens without losing strength, simulating the softening phenomenon caused by the loss of cementitious components within the limestone when exposed to water. Through multiple indoor tests, the final similar material mix was determined as river sand: barite powder: gypsum: polyvinyl acetate: water = 1:0.377:0.245:0.755:0.189. After preparing the samples, soaking tests were conducted to verify whether their deterioration behavior mimicked that of limestone, as shown in Fig. 4a–c. After several preliminary tests, it was determined that the compressive strength of the soaked samples at 0 min, 3 min, 7 min, and 15 min could effectively reflect the degradation of strength, as shown in Fig. 4d. The data were then fitted, and comparisons with literature (Gao et al., 2020; Yan et al., 2022) revealed that the strength degradation pattern of the samples closely matched that of limestone. Furthermore, fitting the data using the limestone strength degradation formula from the literature resulted in a good correlation, indicating that using similar materials to simulate the degradation phenomenon of limestone is feasible.

In selecting materials to simulate the shear band–bedrock interface, a certain amount of polyvinyl acetate is applied to the shear band–bedrock interface to simulate its strength. The amount of polyvinyl acetate used must be meticulously controlled; excessive usage can result in an extended drying period for the model, potentially compromising the integrity of the shear band–bedrock interface and hindering the attainment of the desired strength. This, in turn, could lead to the destabilization of the dangerous rock mass model. Conversely, an insufficient amount of polyvinyl acetate would result in the interface being unable to support the weight of the dangerous rock mass, leading to failure. Therefore, prior to constructing the model, it is imperative to calibrate the amount of polyvinyl acetate. Since the shear band–bedrock interface belongs to the structural plane, direct shear tests are necessary to analyze changes in strength due to the drying and soaking of polyvinyl acetate. Standard disc-shaped samples (61.8 mm in diameter) are fabricated from a material analogous to the dangerous rock mass. The samples are bonded with polyvinyl acetate, and the bonded interface serves as the

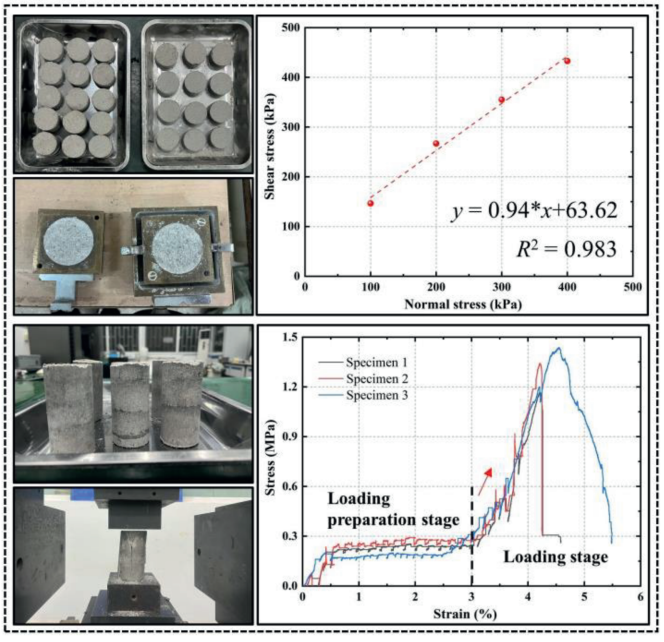


Fig. 3. Preparation of similar materials and acquisition of strength parameters.

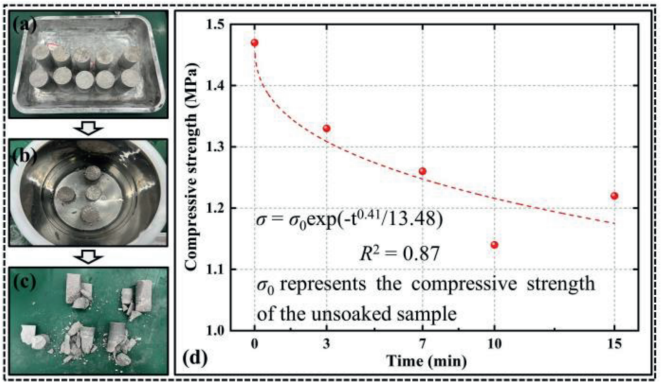


Fig. 4. Degradation of similar materials at different soaking times: (a) Unsoaked sample; (b) Soaked sample; and (c) Broken sample.

Table 2
Similar material parameters.

Value	Density (g/cm^3)	Elastic modulus (GPa)	Compressive strength (MPa)	Poisson's ratio	Cohesion (kPa)	Internal friction angle (°)
Prototype	2.58	13.99	131.7	0.24	5320	44.3
Target	2.58	0.1399	1.317	0.24	53.2	44.3
Actual	2.31	0.1246	1.343	0.22	63.62	43.2

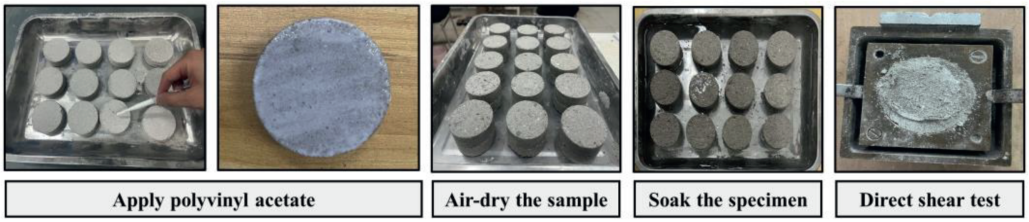


Fig. 5. Preparation of interface materials and acquisition of strength parameters.

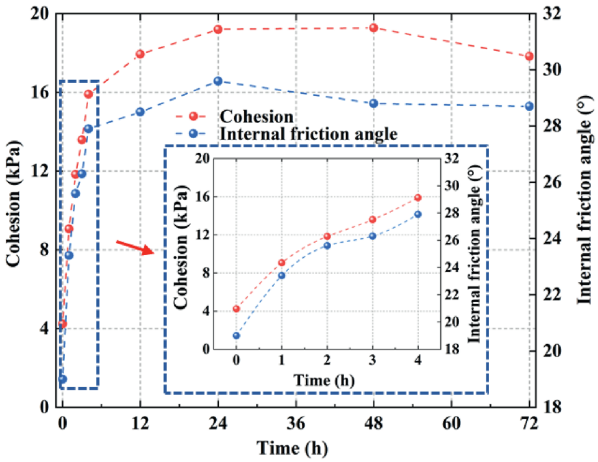


Fig. 6. Drying strength variation curve of interface material.

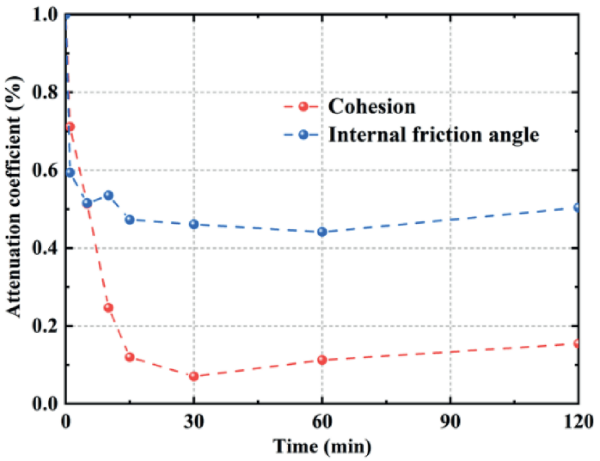


Fig. 7. Degradation curve of strength parameters of interface material.

shear plane. These samples then undergo direct shear testing, as shown in Fig. 5. After the samples are bonded, they are air-dried, and the changes in cohesion and internal friction angle over time are measured, as shown in Fig. 6. The bonding strength of the polyvinyl acetate increases rapidly within the first 4 h and subsequently stabilizes after 12 h. After 72 h, the cohesion reaches 17.83 kPa, and the internal friction angle is 28.7°. Following conversion according to the similarity ratio, the cohesion becomes 1.783 MPa, which is in close agreement with the values reported in the literature (Guo et al., 2025). The degradation curve of the samples upon exposure to water is shown in Fig. 7. During the initial phase of soaking (0–15 min), both the cohesion and internal friction angle of the structural surface decrease rapidly. Eventually, both parameters stabilize and reach a final equilibrium. A comparison of this degradation curve with the trends observed in the literature (Weng et al., 2015; Lo and Weng, 2017; Yan et al., 2022) reveals that the development pattern of this degradation is similar to the actual structural surface degradation. Although the time and values for the water-induced degradation of similar materials cannot be directly correlated with the actual structural plane degradation, this degradation model effectively simulates the failure mode of dangerous rock mass degradation under the influence of reservoir water in the model test (Yan et al., 2022). Through repeated experiments, the optimal amount of polyvinyl acetate to be used was determined to be 0.017 mL/cm^2.

2.4. Model generalization and design

The model of the dangerous rock mass was designed according to a geometric similarity ratio of 1:100, as shown in Fig. 8. The dimensions of the model box are 1 m in length, 0.7 m in width, and 2 m in height. It is constructed from angle steel and steel plates, with a piece of tempered glass on the front to allow for visualization. The model box undergoes strict waterproofing treatment. The bedrock is 86.07 cm long, 50 cm wide, and 175 cm high, with a slope angle of 55° on the bedrock. The cross-sectional shape of the dangerous rock mass is quadrilateral, with a large vertical crack at the rear, extending perpendicularly to the ground. The distance from the slope top to the shear band is 48.8 cm, with a slope angle of 85° and an internal bedding dip of 2°. The model simulates a dangerous rock mass with three sides exposed to water. For the convenience of constructing the model, the internal bedding thickness is set at 2 cm, with a secondary joint spacing of 5 cm. Three vertical cracks are evenly distributed along the HFB surface, with a maximum depth of 5 cm. The model of the dangerous rock mass is shown in Fig. 8a. Liu et al. (2020) summarized five reconstruction modes of the HFB in the TGRA. Field investigations indicate that the HFB of this dangerous rock mass belongs to the collapse-type reconstruction mode. Combining previous research (Liu et al., 2023b), the degradation zone of the HFB rock mass is generalized, with the maximum degradation depth set to 5 cm, as shown in Fig. 8b. Fig. 8c illustrates the generalization model of the shear band. The shear band is divided into dry-wet and non-dry-wet cycle sections, with internal filling material exhibiting layered characteristics. Considering the practical difficulty of cutting the internal filling material of the shear band during construction and the fact that the degree of fragmentation and the thickness of the block inside the shear band do not influence the macroscopic failure mode of the dangerous rock mass, in this test, the internal filling material of the shear band does not need to be broken and is generalized as layered blocks, each 1 cm in length and 1.5 cm in height (the width of the shear band observed in the field ranges from 0.5 m to 1.8 m), with no special cementation between the blocks (Liu et al., 2024).

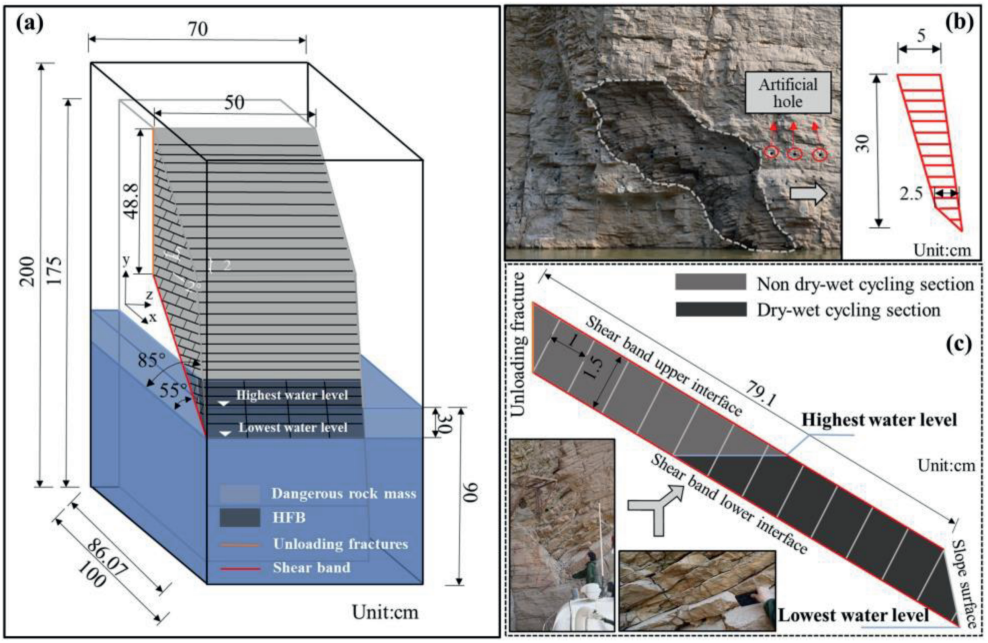


Fig. 8. Schematic diagram of the generalized model of the dangerous rock mass: (a) Dangerous rock mass model; (b) Degradation zone of rock mass in the HFB; and (c) Generalization of the shear band.

2.5. Measuring point layout

To investigate the variation of pore water pressure and stress within the dangerous rock mass under the influence of reservoir water, particular attention should be given to the changes in rock pressure near the trailing edge crack of the dangerous rock mass, on both sides of the shear band and at the intersections of the shear band with the highest water levels. Meanwhile, pore water pressure variations should be monitored within the rock mass located in the HFB and in areas of the dangerous rock mass close to the shear band. Therefore, a total of 10 rock pressure sensors (S1–S10) and 4 pore water pressure sensors (P1–P4) are arranged inside the dangerous rock mass. The specific arrangement is shown in Fig. 9. Among them, sensors S1–S3 are located at the two ends and the middle of a trailing edge crack in the dangerous rock mass. These sensors are oriented vertically to monitor changes in horizontal pressure at their respective positions (the purpose of this arrangement is to compare the stress changes of the dangerous rock mass containing double shear bands when it fails). Sensors S4–S10 (except S8) are placed on both sides of the shear band to monitor changes in vertical pressure at their respective locations. Among these, S4 and S5 are located near the trailing edge crack, S6 and S7 are arranged below the highest water level and close to the water level, and S9 and S10 are installed near the slope toe. S8 is aligned horizontally with S6 and S7, positioned near the surface of the HFB. The pore water pressure sensors P1, P3, and P4 are arranged from top to bottom near the surface of the HFB, monitoring the changes in pore water pressure at the upper, middle, and lower parts of the HFB, respectively. P2 is positioned at a level aligning with P3 and near the shear band, monitoring the pore water pressure at the upper interface of the shear band.

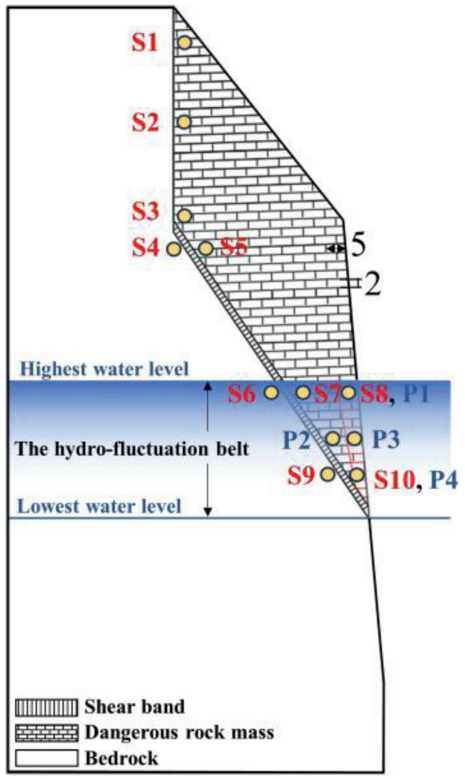


Fig. 9. Measuring point layout plan.

2.6. Model fabrication and testing scheme

Fig. 10 illustrates the process of creating the dangerous rock mass model. The bedrock is constructed using brick and cement mortar to ensure its rigidity and waterproof capabilities. Polyvinyl acetate adhesive is evenly applied to the surface of the bedrock slope, followed by the rapid covering of similar materials to prevent strength reduction due to adhesive drying. The infill material within the shear band is cut with a knife at 1 cm intervals. Plastic wrap is used to simulate the trailing edge crack of the dangerous rock mass, thereby separating the dangerous rock mass from the

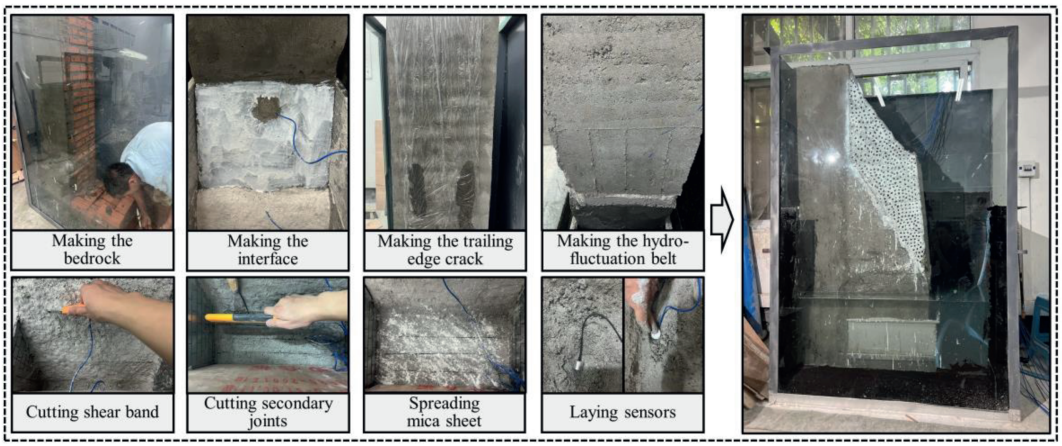


Fig. 10. Making process of the dangerous rock mass model.

bedrock. During the model-making process, filling is carried out from bottom to top. Each layer of rock mass is compacted using a tamper, with a thickness controlled at approximately 2 cm. Secondary joints are then cut, and mica sheets are evenly spread to simulate the rock layer. The vertical fractures in the HFB of the rock mass are created using a slow cutting method. The high water level is aligned with the upper edge of the HFB. Once the dangerous rock mass model is completed, it should be left undisturbed for 2 d to ensure that the bonding material achieves its full strength. After this, the mold is removed, and speckles are applied to the side of the dangerous rock mass to record the displacement changes throughout the failure process.

This experiment is primarily divided into two steps. The first step is water storage, where water is gradually added to prevent the rapid flow from eroding the model and compromising the accuracy of the results. The second step is stabilizing the model, during which the model is left undisturbed, and the maximum water level is maintained. Throughout this process, the water interacts with similar materials, causing internal deformation and stress changes within the dangerous rock mass, thereby simulating the failure process of the rock mass. A data acquisition system – comprising speckle field analysis and stress monitoring instrumentation – is employed to continuously record the variation throughout the entire process.

3. Results analysis

3.1. Failure phenomena of dangerous rock mass

The industrial camera in the XTDIC system was employed to capture the entire process of the dangerous rock mass, i.e. initiation stage – water storage – deterioration – failure, as shown in Fig. 11. The model test can be roughly divided into four stages: the initiation, water storage, the collapse of the rock mass in the HFB, the crack development-penetration, and the failure of the dangerous rock mass. Fig. 11a shows impounding to the lowest water level, corresponding to the 145 m water level of the reservoir, which represents the initial stage of the model test. Fig. 11b presents the stable water at the highest water level, corresponding to the 175 m water level of the reservoir, with the water storage process lasting for a total of 329 s. It can be observed that when the highest water level is reached, the water becomes slightly turbid, possibly due to the reaction between the similar materials and water, with a small amount of particle loss occurring at the slope toe compared to the initiation stage. During the collapse stage of the rock mass in the HFB, as time progresses ($329\ s < T < 1501\ s$; Fig. 11c), the reaction between the shear band and water intensifies. Due to the reduction in strengths of the shear band and interface, localized collapse of the HFB rock mass occurs at the slope toe. This generates cavities at the slope toe, which aligns with the findings obtained from the reconstruction model of the collapse-type HFB rock mass in the reservoir area (Liu et al., 2020). In the crack development-penetration stage ($1501\ s < T < 3560\ s$; Fig. 11d), an upward-inclined crack begins to develop near the boundary between the dry-wet and the non-dry-wet cycle sections of the shear band. This phenomenon is likely due to the internal damage of the dangerous rock mass after the high water level is reached ($T > 329$ s), caused by the loss of shear band fillings and interface strength. As deterioration progresses, fine particles are gradually eroded and transported by seepage, rendering the water increasingly turbid and initiating crack propagation. In the failure stage of the dangerous rock mass ($3560\ s < T < 5297\ s$; Fig. 11e), with the intensification of the deterioration, the cracks near the boundary between the dry-wet and the non-dry-wet

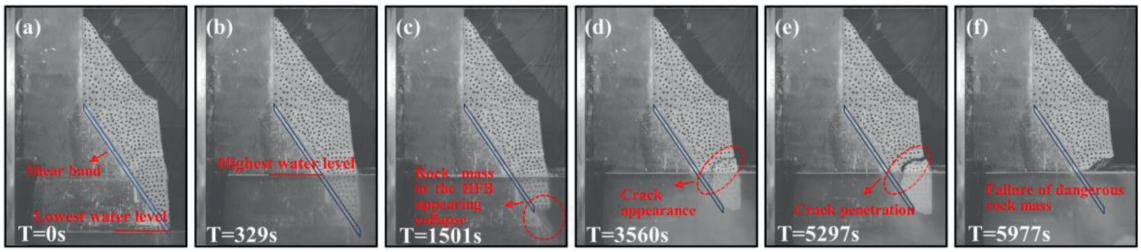


Fig. 11. Failure process of dangerous rock mass: (a) Initiation stage; (b) The moment of reservoir impoundment completion; (c) Collapse stage of the rock mass in the HFB; (d) Crack development stage; (e) Crack penetration stage; and (f) Failure stage.

cycle sections of the shear band gradually connect with the surface cracks of the dangerous rock mass, forming a clearly visible wide crack. This crack cuts and separates the rock mass below it (hereafter referred to as the lower rock) from the parent rock. At this point, the strength of the upper interface of the shear band is almost completely lost, and the lower rock shows significant displacement. At 5297 s < T < 5977 s (Fig. 11f), the upper interface strength of the shear band is entirely lost, causing the lower rock to completely detach from the parent rock and slide downward along the shear band interface, resulting in sliding failure.

Fig. 12 shows photos of the dangerous rock mass after failure. Fig. 12a illustrates the failure phenomenon of the dangerous rock mass after pumping. The cavity in the photo is the location where sensor S9 was embedded. The red area represents the residual shear band, while the blue dashed line indicates the tensile fracture trace after failure. It can be observed that after the lower rock separated from the parent rock, part of the shear band remained, and another part experienced failure. This is because, during the collapse stage of the rock mass within the HFB, the shear band at the slope toe gradually became exposed to water. Due to the absence of cementation between the internal infilled blocks, the likelihood of failure in this section of the shear band significantly increased as deterioration progressed. Combined with the failure phenomena (Fig. 11d, e, and 12a), the lower rock slid along the upper interface between the shear band and the bedrock. Fig. 12b shows the development of the trailing edge crack. After the failure of the dangerous rock mass, the trailing edge crack opened slightly. It is important to note that during the entire test, the deformation of the dangerous rock mass was relatively small, with no obvious displacement traces. However, the speckle field captured the deformation, which will be discussed later. Fig. 12c displays the final failure state of the dangerous rock mass. In summary, the failure mode of dangerous rock masses on bank slopes containing a single shear band can be summarized as follows: collapse of rock mass in the HFB – internal damage to the dangerous rock mass – development and penetration of fractures on both sides of the dangerous rock mass – sliding failure of the lower rock detaching from the parent rock.

3.2. Displacement characteristics of the dangerous rock mass

To explore the displacement characteristics of the slope under the deterioration of reservoir water, the XTDIC technology was used. This technique offers the advantage of capturing continuous deformation of the target body, but it has the limitation of losing part of the speckle field if cracks, large deformations, or a decline in speckle quality occur. The horizontal and vertical displacement fields from water storage to the failure of the dangerous rock mass were obtained, as shown in Figs. 13–15. It is important to note that

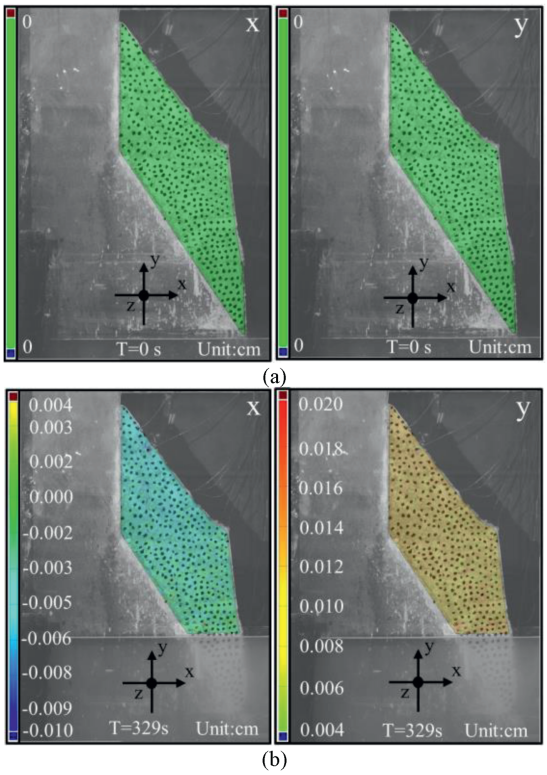


Fig. 13. Displacement characteristics (a) during the initial stage and (b) at the moment of reservoir impoundment completion.

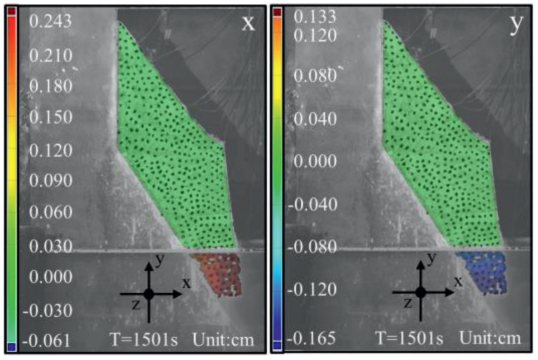


Fig. 14. Displacement characteristics during the collapse stage of the rock mass in the HFB.

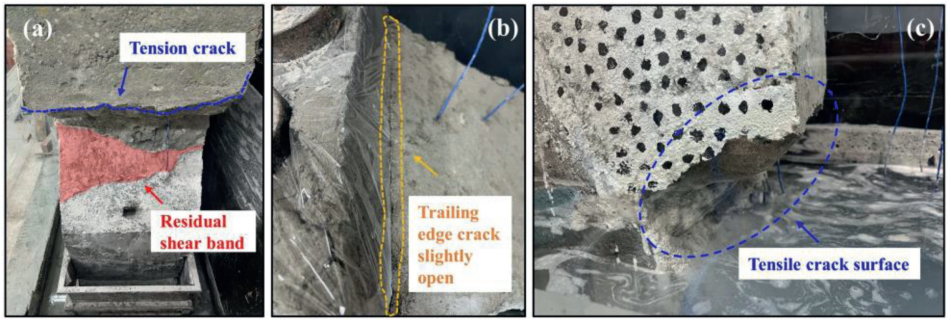


Fig. 12. Final failure phenomenon of the dangerous rock mass: (a) Failure phenomenon of the dangerous rock mass after pumping; (b) Development of the trailing edge crack; and (c) Final failure state of the dangerous rock mass.

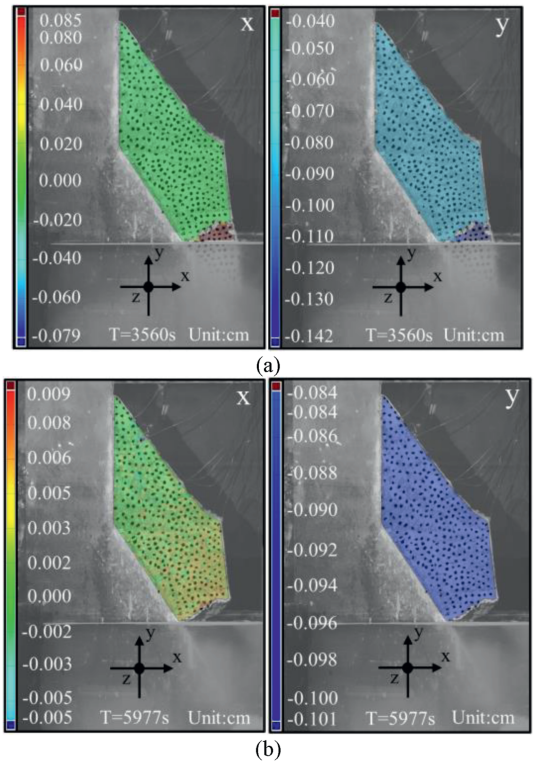


Fig. 15. Displacement characteristics of dangerous rock mass during (a) crack development and (b) failure stages.

at the moment of failure, the speckle field near the cracks is lost, making it impossible to obtain displacement values at that time. Therefore, only the displacement characteristics during the instability process of the dangerous rock mass can be analyzed. The changes in the displacement field are relative values, with the horizontal and vertical displacement values at 0 s taken as the reference. The *x*-axis is defined as positive toward the slope surface from the trailing edge crack, and the *y*-axis is defined as positive upward.

Fig. 13 illustrates the displacement field characteristics of the slope during the initiation–water storage stage and at the moment of reservoir impoundment completion. As shown in Fig. 13a and b, before water storage, both the horizontal and vertical displacements of the slope are zero, and the displacement field within the dangerous rock mass is uniformly distributed. At $T = 329$ s (when water storage is completed), due to the loss of fine particles inside the dangerous rock mass during the water storage process, the water becomes turbid, resulting in the loss of the speckle field below the water surface. Above the water surface, changes in both horizontal and vertical displacements of the slope are observed. From an overall perspective, at this stage, the dangerous rock mass exhibits negative horizontal displacement and positive vertical displacement. This phenomenon can be attributed to the elastic deformation that occurred prior to impoundment, whereby gravitational forces caused a portion of the rock mass to elastically deform relative to the bedrock. During the impoundment process, as the water level gradually rose, partial recovery of this elastic deformation took place, resulting in the monitoring equipment capturing upward and leftward displacements of the dangerous rock mass upon completion of impoundment.

Fig. 14 illustrates the displacement characteristics of the slope during the collapse stage of the rock mass in the HFB. After a period of immersion ($T = 1501$ s), the HFB rock mass collapses and falls from the bottom upward, accompanied by the loss of fillings within the shear band. The changes in the displacement field are primarily concentrated in the rock mass below the water surface, while the deformation of the dangerous rock mass above the water surface remains relatively negligible. In the horizontal direction, the displacement of the HFB rock mass changes from negative to positive, with the magnitude of horizontal displacement gradually decreasing from the slope surface toward the interior, reaching a maximum value of over 0.243 cm. In the vertical direction, the displacement shifts from positive to negative, with the displacement magnitude gradually decreasing from the bottom to the top, reaching a maximum displacement of over 0.165 cm. The horizontal displacement is more prominent compared to the vertical displacement. The observed phenomenon is likely caused by the reduction in interface strength of the shear band and the weakening of the internal filling material. Water infiltration along the shear band interface induces displacement of the HFB rock mass toward the slope surface. Meanwhile, the loss of filling material within the shear band reduces the support of the HFB rock mass, resulting in downward displacement. At this stage, internal damage begins to appear in the dangerous rock mass near the water surface.

Fig. 15 shows the displacement characteristics during the crack development stage (Fig. 15a) and the failure stage of the dangerous rock mass (Fig. 15b). At $T = 3560$ s, after the internal damage of the dangerous rock mass accumulates to a certain threshold, surface cracks appear and gradually penetrate through. At these stages, horizontal displacement of the upper portion of the dangerous rock mass above the water surface remains negligible. However, as the cracks continue to develop and the shear band softens, the dangerous rock mass is dragged downward by the lower rock, resulting in noticeable vertical displacement. The maximum vertical displacement of the upper part of the dangerous rock mass exceeds 0.08 cm, while the maximum vertical displacement of the lower rock surpasses 0.142 cm. The water becomes turbid at this stage, and the lower rock begins to detach from the parent rock. At $T > 5977$ s, the cracks fully penetrate, the shear band loses strength, and the lower rock slides downward along the shear band–bedrock interface. At this moment, the horizontal displacement of the upper part of the dangerous rock mass reaches its maximum at the free face and gradually decreases toward the trailing edge crack, with the maximum displacement ranging between 0.03 cm and 0.05 cm. The dangerous rock mass continues to deform in the negative *y*-axis direction, although the deformation is relatively small, with an incremental displacement of approximately 0.02 cm. This deformation is likely caused by the loss of support from the lower section.

3.3. Stress variation law of dangerous rock mass

Fig. 16 shows the stress variation laws within the slope. Based on the failure phenomena of the dangerous rock mass described in Section 3.1, the stress variation process is divided into five stages: (1) Stage a – Initiation–water storage stage; (2) Stage b – Internal damage and crack formation stage; (3) Stage c – Crack acceleration development stage; (4) Stage d – Crack penetration stage; and (5) Stage e – Dangerous rock mass failure stage. Overall, the stress at measuring points S1–S5 shows little change throughout the process. Significant stress variations are mainly concentrated around the lower rock (i.e. measuring points S6–S10). For measuring point S6, which is located on the bedrock surface below the highest water level, the earth pressure at this point shows almost no change at the beginning of water storage. After the period of water storage, as the strengths of the shear band's internal fillings and interface gradually decrease, the stress at measuring point S6

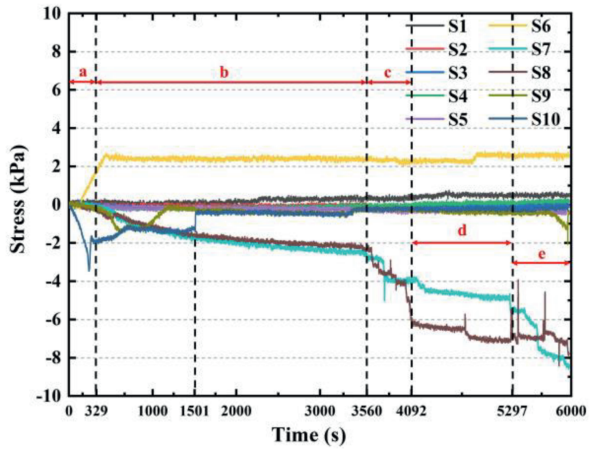


Fig. 16. Variation law of internal stress of slope.

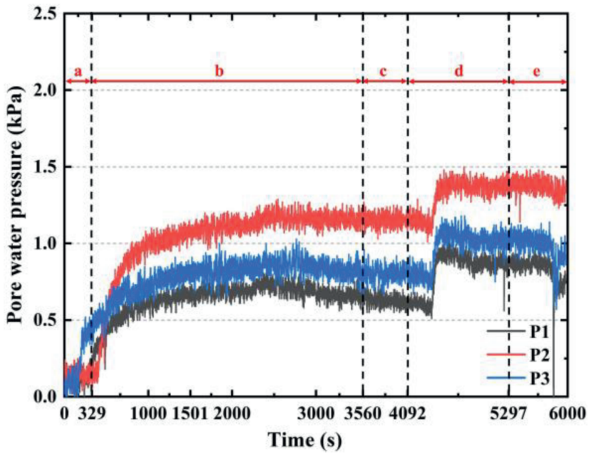


Fig. 17. Variation law of pore water pressure in the HFB.

begins to increase. Following the completion of water storage, the stress at S6 continues to rise. At around 490 s, the stress stabilizes at approximately 2.4 kPa. Although there is a slight increase after 4800 s, the stress value at this point tends to remain stable. The changes at measuring point S6 indicate that as the strengths of the shear band–bedrock interface and the internal filling material deteriorate, the stress at this location gradually increases, showing a compression state. At measuring points S7 and S8, there is a slight decrease in stress during Stage a, but the reduction is minimal. In Stage b, the stress at S7 and S8 gradually decreases, indicating an unloading state. This demonstrates that between 329 s and 3560 s, internal damage begins to accumulate within the dangerous rock mass, creating favorable conditions for subsequent crack development. In Stage c, S7 and S8 experience a sudden stress reduction, coinciding with the initiation of crack development on the external surface of the dangerous rock mass. At this point, a sudden unloading occurs within the lower rock. During Stages d and e, the cracks on the external surface of the dangerous rock mass gradually expand and eventually penetrate through. Since measuring point S8 is closer to the slope surface, the curve indicates that the final amount of unloading at measuring point S7 is greater than that at S8, with a more significant drop in stress. As the lower rock gradually detaches from the parent rock and moves, both measuring points continue to show unloading, indicating that the dangerous rock mass is undergoing failure. For measuring points S9 and S10, since S10 is located at the slope toe, unloading occurs immediately at the beginning of water storage. In contrast, S9, positioned within the bedrock at the slope toe, responds more slowly. During the collapse stage of the HFB rock mass, the unloading at S10 intensifies as the HFB rock mass collapses, gradually losing its overlying earth pressure. After $T > 1501$ s, the rock mass at the slope toe collapses, causing S10 to fall into the water and cease to display earth pressure values. Similarly, S9 also loses its readings due to the collapse of the HFB rock mass. In summary, during the failure process of the dangerous rock mass, as the shear band gradually deteriorates, the stress near the bedrock at the highest water level increases, while a stress reduction occurs within the HFB rock mass near the highest water level. This provides useful insights for monitoring and early warning of such dangerous rock masses.

3.4. Variation law of pore water pressure

Fig. 17 shows the pore water pressure variation curves within the HFB. It is important to note that the sensor at measuring point P4 (located at the slope toe) was damaged during the test; therefore, only the pore water pressure changes at measuring points P1, P2, and P3 are presented. During the water storage stage, measuring point P3, located in the middle of the HFB and near the slope surface, is the first to show changes in pore water pressure, followed by measuring point P1 in the upper part of the HFB, and finally measuring point P2. At this stage, the deteriorating effect of water on the shear band is not yet significant, causing P2 to respond more slowly than the other points. After water storage is completed, due to the degradation of internal fillings and the interface of the shear band, water enters the slope from the shear band–bedrock interface. Consequently, the pore water pressure at measuring point P2 increases rapidly and eventually exceeds that of the other two points. Positioned at the highest water level, P1 consistently registers the lowest pore water pressure. In Stage d, a sudden simultaneous increase in pore water pressure is observed at the three measuring points. This is likely due to the fact that in the crack penetration stage, the lower rock gradually detaches from the parent rock, allowing a large volume of water to rush into the interior of the dangerous rock mass, causing a sudden increase in pore water pressure.

4. Discrete element numerical simulation

4.1. Numeric simulation scheme

Based on the model test, further studies using the discrete element method (UDEC) were conducted. The simulation considers reservoir water level fluctuations and rock mass deterioration. The dry-wet cycling deterioration equations for limestone and the shear band–bedrock interface in the TGRA, as proposed in the literature (Gao et al., 2020; Guo et al., 2025), were embedded into the FISH language. Reservoir water level fluctuations were simulated by varying the pore water pressure between the highest and lowest water levels. The deterioration equations established a relationship between the strength of limestone and the shear band–bedrock interface and the number of dry-wet cycles. This approach was used to investigate the weakening mechanism of the dangerous rock mass under reservoir conditions and to analyze the variations in displacement and stress fields, and fracture evolution patterns of the dangerous rock mass containing a single shear band. Finally, the orthogonal test method and range analysis were applied to determine the sensitivity of different shear band characteristics, such as the height-to-length ratio of the shear band–bedrock interface, shear bandwidth, shear band dip angle,

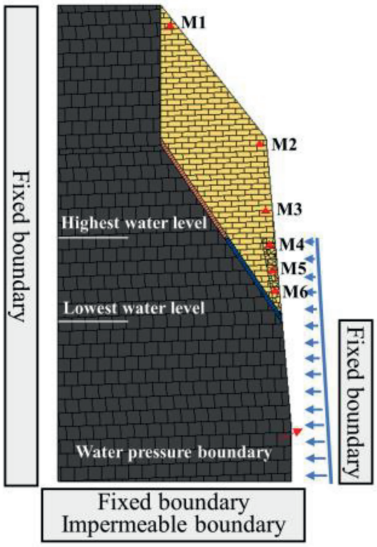


Fig. 18. Boundary conditions and location of monitoring points.

degree of shear band fragmentation, and filling material thickness, on the stability of the slope. The prototype slope model used in the numerical simulation is shown in Fig. 18.

In the numerical model, the fixed boundaries on the left and right sides of the bedrock, a free boundary at the top, and a fixed and impermeable boundary at the bottom are set. The slope top and surface of the dangerous rock mass are assigned free boundaries. A hydraulic gradient is established from the bottom of the bedrock to the highest water level, with the reservoir water level fluctuations simulated by varying the pore water pressure between the highest and lowest water levels. Displacement monitoring points (M1–M6) are placed at the top of the dangerous rock mass, the upper and middle surfaces of the dangerous rock mass, and the upper, middle, and lower surfaces of the HFB rock mass. The discrete blocks adopt a linear elastic constitutive model, while the structural surfaces of the discrete blocks use a contact-Coulomb slip constitutive model. The rock pressure measuring points are positioned at the same locations as in the model test. Notably, the numerical simulation considers the deterioration effect of dry-wet cycles on the rock mass due to reservoir water. The structural surface seepage parameters are set according to previous studies (Liu et al., 2023b; Huang et al., 2025). The selected physical and mechanical parameters of the rock mass, structural plane, and seepage parameters for the numerical simulation are shown in Tables 3–5, respectively.

4.2. Deformation characteristics of dangerous rock mass

4.2.1. Failure process of dangerous rock mass

To visually illustrate the failure process of the dangerous rock mass, displacement cloud maps of the dangerous rock mass after 10, 20, 30, 40, 70, and 90 dry-wet cycles were selected for analysis. Additionally, displacement variation curves in the *x*- and *y*-directions (consistent with the directions described in Section 3.2) were obtained, as shown in Figs. 19 and 20. From the curve, it can be observed that during 0–10 dry-wet cycles, the increases in both horizontal and vertical displacements at each monitoring point on the dangerous rock mass are small. In the model test, this corresponds to the short period following the completion of impoundment, during which the similar material has only just begun to react with water. From the displacement cloud maps, it is evident that the failure mode of the dangerous rock mass in the numerical simulation closely matches that observed in the model test. The dangerous rock mass undergoes a similar process of damage accumulation, crack development and penetration, and eventual detachment of the lower rock from the parent rock. After 10 dry-wet cycles, due to the relatively broken state of the HFB rock mass and the combined effects of high stress from the upper rock mass and the deterioration of both the HFB blocks and joints, displacement changes first appear in the HFB of the dangerous rock mass. At this stage, the deterioration of the shear band–bedrock interface within the dry-wet cycle section remains minor, resulting in negligible overall displacement of the dangerous rock mass. After 20 dry-wet cycles, due to the deterioration of the interface, filling materials, and the HFB rock mass, the entire dangerous rock mass begins to deform. The maximum displacement occurs in the HFB at the slope toe. Differential deformation appears at the boundary between the dry-wet and non-dry-wet cycle sections (this point is defined as the differential deformation point), causing an uneven distribution of deformation within the dangerous rock mass. It should be noted that in the model test, due to limitations in speckle quality and measurement accuracy, small-scale changes in the dangerous rock mass above the water level were not captured. As the number of dry-wet cycles increases, after the 30th cycle, noticeable displacement differences begin to appear near the differential deformation point, accompanied by the continuous accumulation of internal damage. According to the displacement curves, although the displacement changes are slow at this stage, there is a clear trend toward acceleration. During the period from 10 to 30 dry-wet cycles, the deformation at each monitoring point within the dangerous rock mass remains relatively consistent and shows a slow, steady increase. In comparison with the test result (Fig. 14), this stage corresponds to the collapse of the rock mass within the HFB and the internal damage phase of the dangerous rock mass. As the HFB rock mass and the shear band deteriorate, both the horizontal and vertical displacements in the lower part of the dangerous rock mass increase. The maximum displacement of the dangerous rock mass occurs in the HFB. When the number of dry-wet cycles reaches 40, the cracks in both sides of the dangerous rock mass penetrate completely, and the displacement cloud map reveals that the displacement field of the dangerous rock mass is clearly divided into two distinct parts. This is reflected in the curves, where the displacement values of monitoring points above the crack (M 1 and M 2) continue to increase slowly in all directions, while the displacement values at points below the crack (M 3–M 6) show a significant increase. Moreover, as the number of dry-wet cycles continues to rise, the displacement growth rate also increases. In comparison with the test result, this stage corresponds to the crack propagation phase (Fig. 15a), during which side fractures of the dangerous rock mass gradually develop and penetrate through, providing conditions for the subsequent detachment of the lower rock from the parent rock. When the number of dry-wet cycles exceeds 70, the lower rock begins to slide, and the displacement cloud diagram shows that the displacement within the shear band below the highest water level consistently remains smaller than that of the lower rock. This finding corroborates the experimental observation that the lower rock slides along the upper interface between the shear band and the bedrock. In the final displacement changes, in the *x*-direction, measuring point M3 within the lower rock has the largest displacement. Measuring point M6, located at the slope toe in the HFB, shows the maximum displacement among the HFB monitoring points due to the severe deterioration of the rock mass at the slope toe. In contrast, measuring point M4, positioned at the top of the HFB, records the smallest displacement. In the *y*-direction, the displacement of the

Table 3
Rock mass parameters.

Density (g/cm^3)	Bulk modulus (GPa)	Shear modulus (GPa)	Cohesion (kPa)	Internal friction angle (°)	Tensile strength (kPa)
2.58	4.21	3.15	5320	44.3	533

Table 4
Structural plane s parameters.

Structural plane	Normal stiffness (GPa/m)	Shear stiffness (GPa/m)	Cohesion (kPa)	Internal friction angle (°)	Tensile strength (kPa)
Bedding planes	16	12	900	33	60
Second joints	12	9.8	80	38	6
Joints in the HFB	10.8	8.6	6.4	28	3.6
Interface	11	9.2	1134	26	4

Table 5
Seepage parameters of structural planes.

Structural plane	Fluid density (g/cm^3)	Equivalent permeability coefficient (Pa^{-1} s^{-1})	Initial joint aperture (10^{-4})	Residual joint aperture (10^{-4})
Bedding planes Second joints Joints in the HFB Interface	1	83.3	5	2

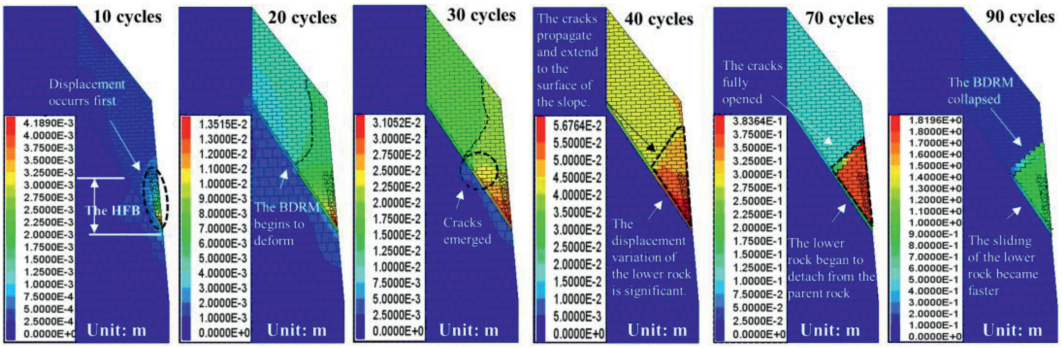


Fig. 19. Failure process of dangerous rock mass in simulation.

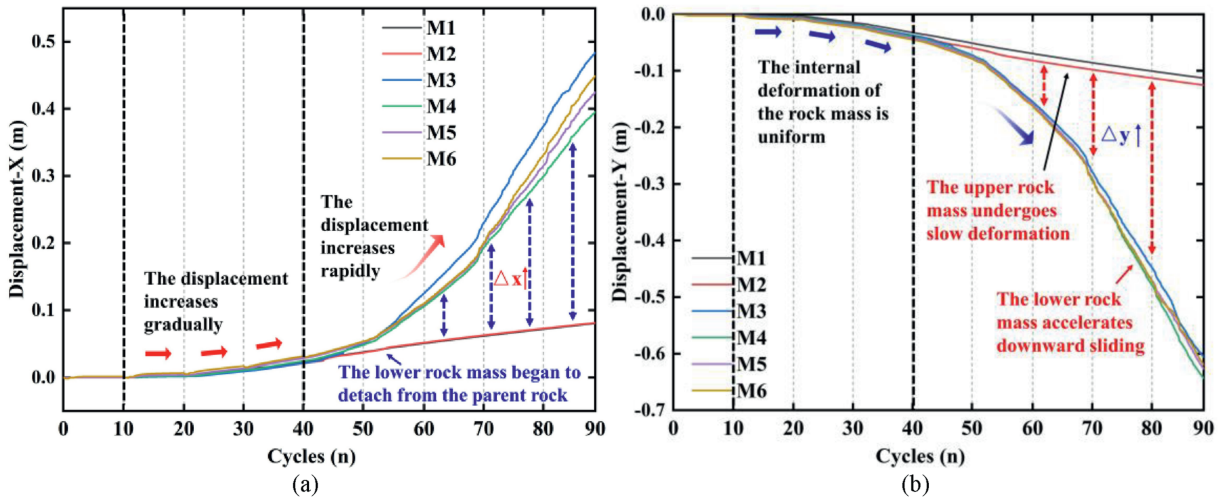


Fig. 20. Displacement variation law of dangerous rock mass: (a) Displacement in the *x*-direction; and (b) Displacement in the *y*-direction.

monitoring points M1 and M2 continues to increase slowly, while the other points, located within the lower rock, exhibit vertical displacements that increase along with the sliding of the lower rock, but the differences in vertical displacement among these points are relatively minor.

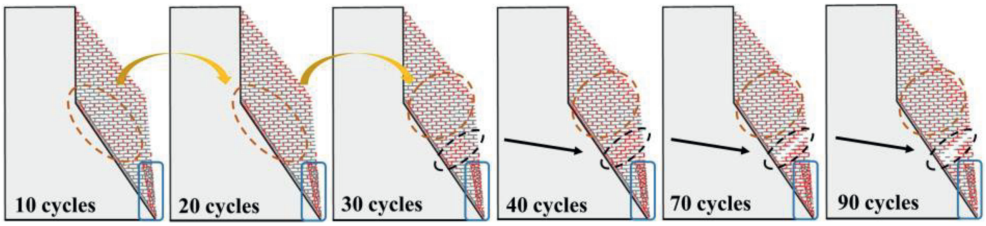


Fig. 21. Evolution of internal cracks in dangerous rock mass.

4.2.2. Evolution law of internal cracks

Fig. 21 illustrates the evolution of internal cracks in the dangerous rock mass at typical dry-wet cycle stages. As shown in the figure, the damage cracks inside the dangerous rock mass are primarily distributed in four areas: the top of the dangerous rock mass, the upper part of the non-dry-wet cycle section of the shear band (highlighted by the yellow dashed box, hereafter referred to as the yellow area for convenience), the vicinity of the highest water level (black area), and the deteriorated zone within the HFB rock mass (blue area). Throughout the failure process of the dangerous rock mass, the distribution of cracks at the top of the dangerous rock mass remains relatively unchanged, while crack development is more significant in other areas. After 10 dry-wet cycles, damage starts to emerge in the yellow area (upper part of the non-dry-wet cycle section of the shear band) and the blue area (deteriorated zone of the HFB), but the damage is not concentrated. The black area (near the highest water level) remains undamaged. Compared to the displacement cloud map (Fig. 19), the displacement of the dangerous rock mass at this stage is minimal, and internal damage remains relatively slight under the effect of 10 dry-wet cycles. After 20 dry-wet cycles, differential deformation occurs at the boundary between the dry-wet and the non-dry-wet cycle sections of the shear band. Cracks begin to develop within the yellow area, and the damaged region expands. In the blue area, cracks develop slightly, while the black area shows no significant changes. When the number of dry-wet cycles reaches 30, cracks in the yellow area begin to develop and gradually connect with the crack zone at the top of the dangerous rock mass. Subsequently, as the number of dry-wet cycles increases, the damage distribution in the upper part of the dangerous rock mass near the highest water level becomes more uniform, and no distinct crack propagation is observed. Meanwhile, the rock mass in the HFB continues to deteriorate, with joint damage intensifying. It should be noted that in UDEC, the collapse of the HFB rock mass observed in the model test does not occur. This is because large displacements of blocks would cause the model to become non-convergent and terminate. However, in the numerical simulation, significant crack propagation occurs in the HFB. In the black area, cracks develop and gradually extend toward the free face. The starting point of these cracks is located precisely near the differential deformation point. Between 40 dry-wet cycles and the failure stage, it is evident that cracks in the black area gradually expand and eventually penetrate, cutting the dangerous rock mass into two parts. Meanwhile, the cracks and damage in the HFB continue to worsen, leading to the detachment of the lower rock from the parent rock and subsequent sliding failure along the upper interface of the shear band. In summary, before 40 dry-wet cycles, internal damage appears within the dangerous rock mass, and cracks begin to develop and propagate. After 40 dry-wet cycles, cracks at the highest water level gradually penetrate, while the HFB rock mass becomes increasingly broken with the rising number of dry-wet cycles.

4.3. Variation characteristics of the stress field

Fig. 22 shows the internal stress field variation of the dangerous rock mass at typical dry-wet cycle stages, and the locations of the stress monitoring points are identical to those in the model test. Fig. 23 presents the stress variation curves of measuring points S6–S8 in the numerical simulation (with values on the curve shown as relative values). As shown in the figures, after 10 dry-wet cycles, the overall internal stress field of the dangerous rock mass remains relatively uniform, with minimal pressure changes observed at each measuring point. The stress distribution is stable, and no significant stress concentration is detected. After 20 dry-wet cycles, stress changes become noticeable near the differential deformation point in the bedrock. Internal damage occurs near this point, resulting in rock mass unloading. At this stage, stress concentration appears at measuring point S6, while measuring points S7 and S8 show a decline in stress values. After 30 dry-wet cycles, the unloading area near the differential deformation point gradually expands and connects with the low-stress zone at the top of the dangerous rock mass. Comparing this with the crack propagation map, cracks at the highest water level begin to appear and gradually expand at this stage. The pressure at measuring point S6 continues to rise, while S7 and S8 experience further stress reduction. From 40 dry-wet cycles to the failure of the dangerous rock mass, cracks gradually develop and reach the slope surface. The lower rock loses its overlying pressure, leading to a general decrease in internal stress, and the unloading zone continues to expand. Since the cracks are completely penetrated, the stress at S7 and S8 gradually stabilizes, and S6 no longer shows a significant increase in stress. Notably, after 40 dry-wet cycles, S6 briefly exhibits a drop in stress followed by a return to stability. This short-term decrease is likely caused by the momentary unloading due to crack opening. By comparing the stress variation curves at each monitoring point from the numerical simulation and the model test, it is observed that the stress at point S6 gradually increases and eventually stabilizes before the 40 dry-wet cycles. This trend aligns with the result prior to the end of the internal damage and crack appearance stage. Similarly, in the numerical simulation, the stress values at points S7 and S8 show a gradual decrease followed by stabilization before the 40 dry-wet cycles, which is also consistent with the trend observed in the model test prior to the end of the internal damage and crack appearance stage. In summary, before 40 dry-wet cycles, internal stress changes in the dangerous rock mass are quite significant. Stress concentration occurs near the differential deformation point, while rock mass unloading is observed in the vicinity of the highest water level.

4.4. Sensitivity analysis of influential factors of shear band characteristics to the stability of dangerous rock mass

The characteristics of the shear band play a crucial role in the stability of dangerous rock masses containing shear bands. In this

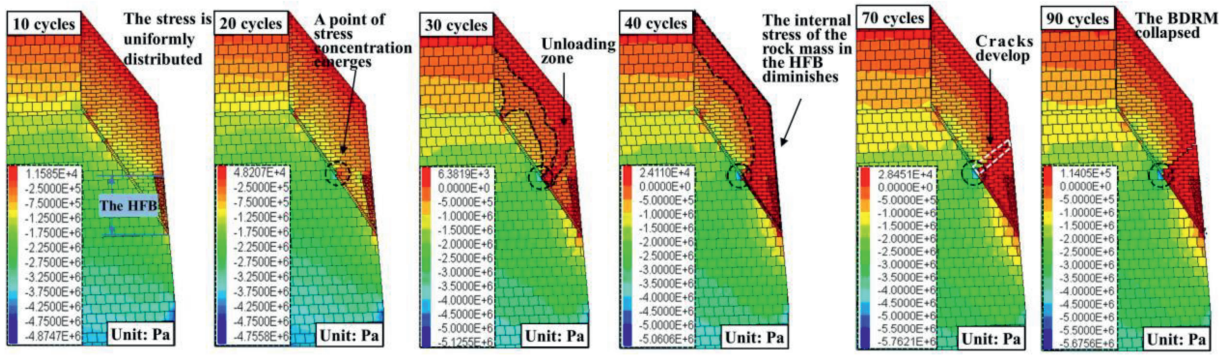


Fig. 22. Variation characteristics of the stress field in the dangerous rock mass.

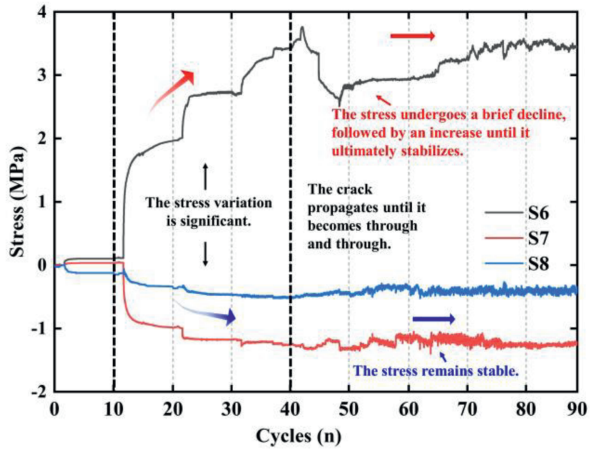


Fig. 23. Variation curves of the stress at measuring points S6–S8 in simulation.

Table 6
Orthogonal test scheme and results.

No.	*A*	*B* (m)	*C* (°)	*D*	*E* (m)	Stability coefficient
1	0.1	1	45	d_1	0.5	0.752
2	0.1	1	55	d_2	1.5	0.831
3	0.1	1.5	45	d_3	1.5	0.837
4	0.1	1.5	65	d_1	1	0.496
5	0.1	2	55	d_3	1	0.727
6	0.1	2	65	d_2	0.5	0.344
7	0.3	1	45	d_3	1	0.853
8	0.3	1	65	d_1	1.5	0.806
9	0.3	1.5	55	d_2	1	0.822
10	0.3	1.5	65	d_3	0.5	0.758
11	0.3	2	45	d_2	1.5	0.828
12	0.3	2	55	d_1	0.5	0.791
13	0.45	1	55	d_3	0.5	0.891
14	0.45	1	65	d_2	1	0.925
15	0.45	1.5	45	d_2	0.5	0.847
16	0.45	1.5	55	d_1	1.5	0.869
17	0.45	2	45	d_1	1	0.831
18	0.45	2	65	d_3	1.5	0.953

study, the key shear band characteristics include the height-to-length ratio of the shear band–bedrock interface (*A*), shear band-width (*B*), shear band dip angle (*C*), degree of shear band fragmentation (*D*), and filling material thickness (*E*). The height-to-length ratio of the shear band–bedrock interface is defined as the ratio of the step height to the step length of the interface (Liu et al., 2024). Identifying the sensitivity of these different shear band characteristics to the stability of such dangerous rock masses is essential for effective prevention and control strategies. Orthogonal testing is an efficient method for addressing multi-factor, multi-level problems. Based on the principles of orthogonal testing and referring to relevant studies (Zeng, 2022; Guo et al., 2025), an orthogonal scheme was designed with five factors (the five shear band characteristics) and three levels for each factor. Using UDEC numerical simulation software, stability coefficients were calculated for the dangerous rock mass under different combinations of factors and levels. The intuitive analysis method was applied to rank the sensitivity of each shear band characteristic to the stability of the dangerous rock mass. The results are presented in Tables 6 and 7 and Fig. 24. The stability coefficient was selected based on its value at the moment of failure of the dangerous rock mass. The degree of fragmentation of the shear band is classified as follows: d_1 denotes that no fractures occur in each layer of filling material; d_2 denotes that each layer is cut by 1–2 vertical fractures; and d_3 denotes that each layer is cut by 2–3 vertical fractures.

As shown in Table 7 and Fig. 24, under the deterioration of reservoir water, the sensitivity of different shear band

Table 7
Intuitive analysis results.

Factor	*A*	*B*	*C*	*D*	*E*
Level 1	0.665	0.843	0.825	0.758	0.731
Level 2	0.81	0.772	0.822	0.766	0.776
Level 3	0.886	0.746	0.714	0.837	0.854
Range	0.222	0.097	0.111	0.079	0.124
Order	1st	4th	3rd	5th	2nd

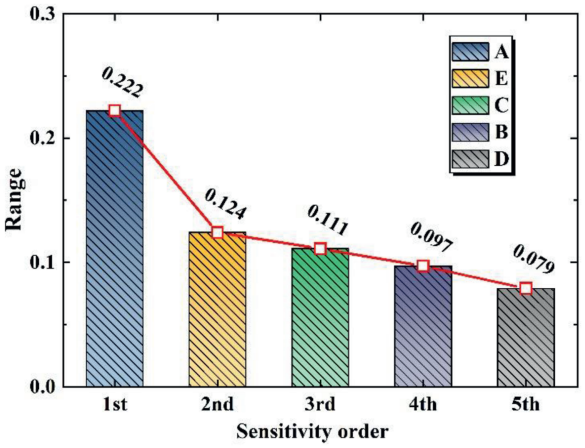


Fig. 24. Sensitivity analysis results.

characteristics to the stability of the dangerous rock mass is ranked as follows: height-to-length ratio of the shear band–bedrock interface (A) > filling material thickness (E) > shear band dip angle (C) > shear bandwidth (B) > degree of shear band fragmentation (D). The sensitivity of the height-to-length ratio of the shear band–bedrock interface (A) is significantly higher than that of the other four factors, indicating that the morphological characteristics of the shear band–bedrock interface have the most pronounced impact on the stability of the dangerous rock mass. The sensitivity of filling material thickness (E) is slightly greater than that of the shear band dip angle (C), followed by the shear bandwidth (B), while the degree of shear band fragmentation (D) exhibits the lowest sensitivity. This result confirms that the shear band–bedrock interface and internal filling material are critical factors affecting the stability of the dangerous rock mass. Moreover, the deterioration effect of reservoir water on these two factors is a crucial issue that must not be overlooked when monitoring the stability of the dangerous rock mass. These findings provide a valuable reference for the stability evaluation and mitigation of similar dangerous rock masses.

5. Conclusions

Through field investigations and laboratory model tests, the failure mode, displacement characteristics, internal stress variation, and pore water pressure evolution of dangerous rock masses containing a single shear band under the deterioration of reservoir water were clarified. Combined with discrete element numerical simulations, the displacement field, internal crack evolution, and stress field changes of dangerous rock masses under the influence of reservoir water were obtained. Finally, the orthogonal test method was employed to determine the sensitivity of different shear band characteristics to slope stability. The main conclusions are as follows.

(1) Under the deterioration of reservoir water, during the initiation–water storage stage, both the vertical and horizontal displacements of the dangerous rock mass are negative. In the collapse stage of the HFB rock mass, the horizontal displacement decreases from the slope surface toward the interior, while the vertical displacement gradually decreases from the lower to the upper part of the slope. Internal damage begins to develop within the dangerous rock mass. At the highest water level, cracks develop on both sides of the dangerous rock mass and propagate diagonally upward. After the cracks penetrate, the lower rock detaches from the parent rock and undergoes sliding downward along the upper interface of the shear band–bedrock boundary. The failure mode of dangerous rock masses on bank slopes containing a single shear band can be summarized as follows: collapse of rock mass in the HFB – internal damage to the dangerous rock mass – development and through-going of fractures on both sides of the dangerous rock mass – sliding failure of the lower rock detaching from the parent rock.

(2) Throughout the failure process of the dangerous rock mass, as the shear band gradually deteriorates, the stress near the bedrock at the highest water level increases, while the internal stress within the HFB rock mass near the highest water level decreases. The change in pore water pressure at the shear band–bedrock interface is slower than that within the HFB rock mass. However, as the deterioration intensifies, the pore water pressure at the interface eventually exceeds that inside the HFB rock mass.

(3) In the numerical simulation, under the deterioration of reservoir water, the displacement of the dangerous rock mass shows a slow increase before 40 dry-wet cycles. Internal damage zones are primarily concentrated in the rock mass at the highest water level. Stress concentration gradually appears near the differential deformation point inside the dangerous rock mass. After 40 dry-wet cycles, the horizontal and vertical displacements on the parent rock surface increase, but the growth rate remains slow. In contrast, the horizontal and vertical displacements of the lower rock increase rapidly. Cracks develop on both sides of the dangerous rock mass and gradually penetrate, ultimately causing the lower rock to detach from the parent rock. The bedrock near the highest water level remains in a compressed state with minimal stress changes, while rock mass unloading occurs within the lower rock. The HFB rock mass becomes increasingly broken as the number of dry-wet cycles increases.

(4) Under the deterioration of reservoir water, the sensitivity of different shear band characteristics to the stability of the dangerous rock mass is ranked as follows: height-to-length ratio of the shear band–bedrock interface > filling material thickness > shear band dip angle > shear band width > degree of shear band fragmentation. The morphological characteristics of the shear band–bedrock interface have the most significant impact on the stability of the dangerous rock mass. The deterioration of the shear band–bedrock interface and internal filling material is the key factor influencing the stability of the dangerous rock mass.

(5) In practical engineering, the instability risk of such dangerous rock masses can be assessed and predicted by comprehensively analyzing the stress variations at the intersection of the highest water level and the bedrock, as well as within the rock mass in the HFB, alongside the development of lateral cracks and the expansion of the trailing edge cracks. By analyzing the sensitivity of the dangerous rock mass stability to the characteristics of the shear band, the degree of deterioration at different positions along the shear band can be refined. Combined with deep learning algorithms, these findings are expected to offer a theoretical foundation for quality evaluation of the shear band deterioration zone.

CRediT authorship contribution statement

Xueyan Guo: Writing – review & editing, Writing – original draft, Methodology, Formal analysis, Data curation. **Xinrong Liu:** Writing – review & editing, Supervision, Project administration, Funding acquisition, Conceptualization. **Jilu Zhang:** Writing – review & editing, Validation, Investigation, Formal analysis. **Lojain Suliman:** Writing – review & editing, Visualization, Methodology. **Xinyang Luo:** Writing – review & editing, Software, Investigation. **Fuchuan Zhou:** Writing – review & editing, Supervision.

Data availability statement

Data supporting this research article are available from the corresponding author on request.

Declaration of competing interest

The authors declare that they have no known competing financial interests or personal relationships that could have appeared to influence the work reported in this paper.

Acknowledgements

This study was jointly funded by the Chongqing Talents and Outstanding Scientists Project (Grant No. cstc2024ycjh-bgzxm0032), National Natural Science Foundation of China (Grant No. 41972266), and Chongqing Natural Science Foundation (Grant No. CSTB2024NSCQ-MSX0006). In addition, we are deeply grateful to Dr. Lojain Suliman for reviewing the manuscript for grammatical and spelling accuracy.

References

Chen, W., Xu, Z.M., Liu, W.L., 2015. Mechanical model and failure mechanism of unstable cantilevered rock blocks due to differential weathering. Rock Soil Mech. 36 (1), 195–204 (in Chinese).

Chen, Y.F., Zhang, P., Huang, B.L., Qin, P., Li, Q., 2022. Failure process and long-term stability analysis of typical unstable rock mass in the three gorges reservoir area considering rock mass deterioration. J. Geom. 28 (6), 938–947.

Elkamhawy, E., Wang, H.B., Zhou, B., Yang, Z., 2018. Failure mechanism of a slope with a thin soft band triggered by intensive rainfall. Environ. Earth Sci. 77 (9), 340.

Fan, Y.J., Yang, G.X., Ye, H.L., Liu, Y., 2024. Seismic response investigation of pre-stressed anchor cable supporting rock slope with weak interlayer in Qinghai Tibet Plateau, China. Sci. Rep. 14 (1), 18088.

Fu, Y., 2011. Study on water–rock Interaction with the Cyclic drying-wetting Effect on Rock. PhD Thesis. Chongqing University, Chongqing, China (in Chinese).

Gao, X.C., Gu, D.M., Huang, D., Zhang, W.G., Zheng, Y., 2020. Development of a DEM-based method for modeling the water-induced failure process of rock from laboratory- to engineering-scale. Int. J. GeoMech. 20 (7), 04020080.

Guo, J., 2021. Research on the Instability Process of Tower Rocks Under the Fluctuation Levels of Water Reservoirs. MSc Thesis. China Three Gorges University, Yichang, China (in Chinese).

Guo, X.Y., Lojain, S., Liu, X.R., Luo, X., Zhou, F., Wang, H., Wang, G., 2025. Damage evolution characteristics of the shear band-bedrock interface under dry-wet cycling: experimental and numerical simulation. J. Mt. Sci. 22, 3869–3886.

Huang, X.C., Wang, G.L., Zhang, L.L., 2025. An analytical solution for critical sliding surface of stepped rock slope: a case study of Xinjing coal mine landslide. Bull. Eng. Geol. Environ. 84 (2), 78.

Hungr, O., Leroueil, S., Picarelli, L., 2014. The Varnes classification of landslide types, an update. Landslides 11 (2), 167–194.

Li, Z.C., Zhang, H., Cheng, P.F., Wang, Y.L., 2024. Experimental study on the development process and spatial distribution of shear band of coarse-grained sliding zone soil. Rock Soil Mech. 45 (4), 1067–1080 (in Chinese).

Liu, X.R., Guo, X.Y., Xu, B., Zhou, X.H., Zeng, X., Xie, Y.K., Wang, Y., 2023a. Investigation on dynamic cumulative damage mechanism of the dangerous rock slope including deteriorated rock mass in hydro-fluctuation belt. Rock Soil Mech. 44 (3), 637–648 (in Chinese).

Liu, X.R., Guo, X.Y., Zhou, X.H., Luo, X., Wang, H., Li, P., Zhou, F., 2024. Study on macro-meso shear transfixion mechanism and mechanical properties of shear band-bedrock interface of dangerous rock on reservoir bank. Chin. J. Rock Mech. Eng. 43 (5), 1096–1109 (in Chinese).

Liu, X.R., Jing, R., Miao, L.L., Han, Y.F., Deng, Z.Y., Xiong, C., 2020. Reconstruction models and typical case analysis of the fluctuation belt of reservoir bank slopes in Wushan. Chin. J. Rock Mech. Eng. 39 (7), 1321–1332 (in Chinese).

Liu, X.R., Luo, X.Y., Guo, X.Y., Zhou, X.H., Wang, H., Xu, B., Zheng, Y.R., 2025. Water–rock degradation characteristics and dangerous rock failure modes in wushan bank slope. J. Eng. Geol. 33 (1), 240–257 (in Chinese).

Liu, X.R., Wang, Y., Xu, B., Zhou, X., Guo, X., Miao, L., 2023b. Dynamic damage evolution of bank slopes with serrated structural planes considering the deteriorated rock mass and frequent reservoir-induced earthquakes. Int. J. Min. Sci. Technol. 33 (9), 1131–1145.

Lo, C.M., Weng, M.C., 2017. Identification of deformation and failure characteristics in cataclinal slopes using physical modeling. Landslides 14 (2), 499–515.

Shi, A.C., Xie, M.W., Zhao, L.Y., Zhang, X.Y., Wu, Z.X., Wu, S.M., 2023. Experimental study of single structure surface dangerous rock mass dynamic characteristics based on constant micromotion. Adv. Civ. Eng. 2023, 2869772.

Shi, C., Yang, B., Zhang, Y.P., Yang, J.X., 2020. Application of discrete-element numerical simulation for calculating the stability of dangerous rock mass: a case study. Int. J. GeoMech. 20 (12), 04020231.

Wang, L.F., Zhang, J.X., Huang, X.M., Tan, G.J., 2023. Study on the dynamic stability and spectral characteristics of a toppling dangerous rock mass under seismic excitation. Sustainability 15 (21), 15397.

Wang, L.Q., Yin, Y.P., Huang, B.L., Zhang, Z., Zhao, P., Wei, Y., 2020b. A study of the treatment of a dangerous thick submerged rock mass in the three gorges reservoir area. Bull. Eng. Geol. Environ. 79 (5), 2579–2590.

Wang, L.Q., Yin, Y.P., Huang, B.L., Dai, Z.W., 2020a. Damage evolution and stability analysis of the jianchuandong dangerous rock mass in the three gorges reservoir area. Eng. Geol. 265, 105439.

Wang, X., Fu, X.D., Wu, K., Ding, H., Du, W., Sheng, Q., Chen, J., 2024. Analysis of historical evolution characteristics and collapse process on July 18, 2023, of a dangerous rock mass at Guanyinyan in Baoxing County, Sichuan Province, China. Landslides 21 (6), 1367–1383.

Wei, L.T., Xu, Q., Wang, S.Y., Wang, C., Ji, X., 2020. The morphology evolution of the shear band in slope: insights from physical modelling using transparent soil. Bull. Eng. Geol. Environ. 79 (4), 1849–1860.

Weng, M., Lo, C., Wu, C.H., Chuang, T.F., 2015. Gravitational deformation mechanisms of slate slopes revealed by model tests and discrete element analysis. Eng. Geol. 189, 116–132.

Xu, B., Liu, X.R., Zhou, X.H., et al., 2022. Investigation on the dynamic cumulative damage mechanism and stability of bedding rock slope under the deterioration of rock mass in the hydro-fluctuation belt. Bull. Eng. Geol. Environ. 81 (8), 332.

Yan, G.Q., Yin, Y.P., Huang, B.L., Hu, L., 2022. Research on deterioration-buckling failure mechanism of consequent bedding limestone bank slope in Three Gorges Reservoir Area. Rock Soil Mech. 43 (9), 2568–2580 (in Chinese).

Yin, Y.P., Wang, L.Q., Huang, B.L., Zhang, Z., Dai, Z., 2023. Evolution analysis of the Banbiyan dangerous rock mass in the Three Gorges Reservoir area, China. Georisk 17 (2), 376–386.

Yin, Y.P., Wang, L.Q., Zhao, P., Zhang, Z.H., Huang, B.L., Wang, X.B., 2022. Crashed failure mechanism and prevention of fractured high-steep slope in the Three Gorges Reservoir, China. J. Hydraul. Eng. 53 (4), 379–391 (in Chinese).

Zeng, X., 2022. Study on Dynamic Response Characteristics and Stability of Typical Dangerous Rock Mass Along the Three Gorges Reservoir. MSc Thesis. Chongqing University, Chongqing, China (in Chinese).

Zhao, Z.N., Li, B., He, K., Yin, Y.P., Gao, Y., 2022. Fracture mechanical analysis of collapse down of columnar dangerous rock base in southwest mountainous area. Chin. J. Rock Mech. Eng. 41 (Suppl. 2), 3132–3140 (in Chinese).

Zheng, A.X., Luo, X.Q., Shen, H., 2013. Numerical simulation and analysis of deformation and failure of jointed rock slopes by extended finite element method. Rock Soil Mech. 34 (8), 2371–2377 (in Chinese).

Zhou, F.C., Tang, H.M., Chen, S., Wang, L., Shang, C., 2023. Research on the damage-catastrophe mechanism of a tower-column unstable rock mass with compressed-fracture slumping mode under multi-factor couplings. Geotech. Geol. Eng. 41 (1), 135–151.



Xueyan Guo obtained his MSc degree in 2021 from Southwest Jiaotong University, majoring in civil engineering. His research during that period focused on the stability of deposit slopes under strong seismic loading. He is now pursuing a PhD in geotechnical engineering at Chongqing University, where his work primarily explores the degradation mechanisms of rock masses in the hydro-fluctuation belt in the Three Gorges Reservoir area, as well as the static and dynamic stability of dangerous rock masses.